Monolithically-Integrated Nested Ridge Waveguide Dual-Channel Filters

Berkay Dogan[1#*], Dimitra Psychogiou[2#*]

Tyndall National Institute[#], University College Cork*, Ireland
[1]berkay.dogan@tyndall.ie, [2]DPsychogiou@ucc.ie

***Abstract* — This paper presents a novel highly-miniaturized dual-channel 3D filter design concept. It is based on a new nested waveguide resonator approach that allows the excitation of two fully-isolated fundamental resonances within the volume of a conventional ridge waveguide. Size compactness is achieved by: i) re-using traditionally unused areas of a ridge waveguide and ii) monolithic integration enabled by stereolithography apparatus 3D printing. A novel ridge-waveguide/waveguide (RW-WG) resonator concept is proposed and analysed in detail for the realization of two-channel filters. For proof-of-concept validation purposes, a dual-channel RW-WG-based bandpass filter (BPF) was designed, manufactured and tested. It exhibits a second order low frequency filtering channel at 6.77 GHz with minimum in-band insertion loss (IL) of 0.16 dB (Q_{eff} of 1,060) and 3 dB fractional bandwidth (FBW) of 7%, and a second order high-frequency filtering channel at 15.39 GHz with minimum IL of 0.2 dB (Q_{eff} of 1,365) and 3 dB FBW of 5.3%.**

***Keywords* — additive manufacturing (AM), bandpass filter, dual-channel filter, monolithic integration, ridge waveguide, stereolithography apparatus (SLA), 3D printing.**

I. Introduction

Recent advances in emerging wireless applications such as vehicle-to-vehicle (V2V) connectivity, internet-of-space (IoS) and 5G+ communications are increasingly calling for RF transceivers able to support higher bandwidths (BWs), higher data rates, and multiple applications. Addressing these needs using conventional RF front-ends (RFFEs) results in high levels of complexity and large size, due to needing to use dedicated transmitter/receiver chains for each application [1], [2]. As one of the most fundamental elements, RF filters dictate the RFFE size when low loss or high-power handling is required, for example in the case of RFFEs for base station or satellite systems. These require high unloaded quality factor (Q) resonators that can only be realized using air-filled 3D cavities which are bulky and heavy [3]. To facilitate size compactness, recent research efforts are geared towards miniaturization using dual-mode air-filled resonators where two degenerate modes are excited within a single cavity [4], [5]. Miniaturization using high-permittivity dielectric-filled metallic resonators have also been reported [6].

Size constraints become even more critical when attempting to realize multi-channel RFFEs. In [7], a multi-channel 3D bandpass filter (BPF) design approach using mode-composite ridge-loaded cavity resonators is discussed. They are built using multi-part CNC machining leading to passbands with IL of about 0.9 dB; however, their bands cannot be independently controlled. For miniaturization in multi-channel filters, dual-mode dielectric resonators are proposed [8] for architectures with 2-12 channels [9]. However, their passbands have moderate IL of about 1 dB, and low channel isolation of about 30 dB.

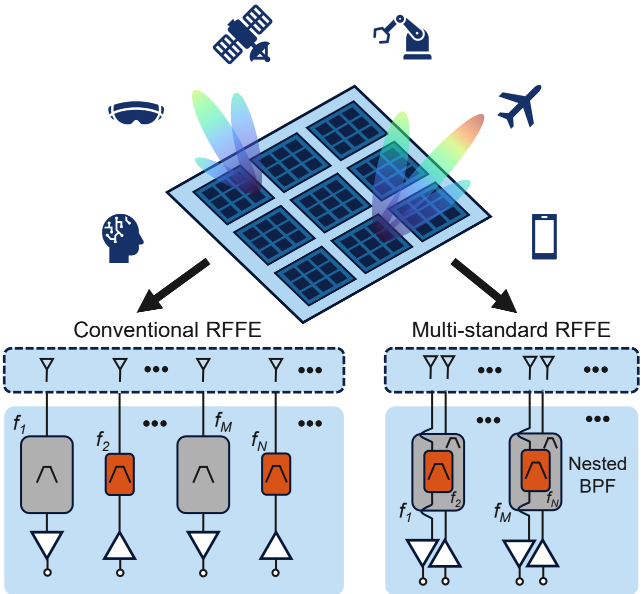

(a) (b)

Fig. 1. Multi-standard antenna front-end interface supporting multiple communication bands/channels. (a) Conventional RFFE approach using dedicated filters for each band/channel. (b) Proposed RFFE having a reduced number of filters using the proposed nested RW-WG BPF concept.

To facilitate size compactness and weight reduction in 3D RF components, alternative digital additive manufacturing techniques such as stereolithography apparatus (SLA), digital metal laser sintering (DMLS) are increasingly explored for monolithic, low weight RF filters and diplexers. Alternative integration concepts using spherical [10], capacitively-loaded hemispherical resonator [11] and 3D ellipsoidal [12] resonators have been explored. However, most of them have been used for single-ended BPFs and none of these concepts was applied to multi-channel filters.

Considering the aforementioned limitations, a new 3D printed nested waveguide (WG) resonator approach is proposed for monolithic highly-miniaturized dual-channel BPFs. It allows the excitation of two fully-isolated fundamental modes within the volume of a conventional ridge waveguide (RW). In this manner, two independent filtering channels can be created within a nested filter that can be used to miniaturize the size of a multi-standard RFFE, for example the one shown in Fig. 1. Size compactness is achieved by: i) re-using traditionally unused areas of a RW resonator and ii) monolithic integration enabled by SLA-based 3D printing. For experimental validation purposes, a dual channel prototype was designed, manufactured and tested for frequency channels within the FR1 (0.41-7.125 GHz) and FR3 (7.125-24.25 GHz) band. It exhibits a second order low frequency filtering channel (LFFC) at 6.77 GHz with minimum in-band IL of 0.16 dB (Q_{eff} of 1,060) and 3 dB fractional bandwidth (FBW) of 7%, and a second order high-frequency filtering channel (HFFC) at 15.39 GHz with minimum IL of 0.2 dB (Q_{eff} of 1,365) and 3 dB FBW of 5.3%.

II. Theoretical Foundations

The key enabling element of the proposed dual-channel BPF concept is the nested ridge-waveguide/waveguide (RW-WG) resonator as shown in Fig. 2. In this case, the traditionally unused area of a RW resonator is used to create a hollow WG resonator allowing for an additional fundamental mode to be excited at a frequency $f_{WG,1}$ while the fundamental mode of the RW resonator will be at a frequency $f_{RW,1}$.

To better explain the design process, the metric achievable frequency ratio (AFR) is defined as the ratio between the two fundamental frequencies $= f_{WG,1}/f_{RW,1}$. It is used for an example design case where the LFFC will be set at 6.75 GHz and the HFFC at 15.375 GHz, leading to a targeted AFR equal to 2.27. Considering this AFR as a reference, geometric parametric studies are performed for the fundamental modes of each of

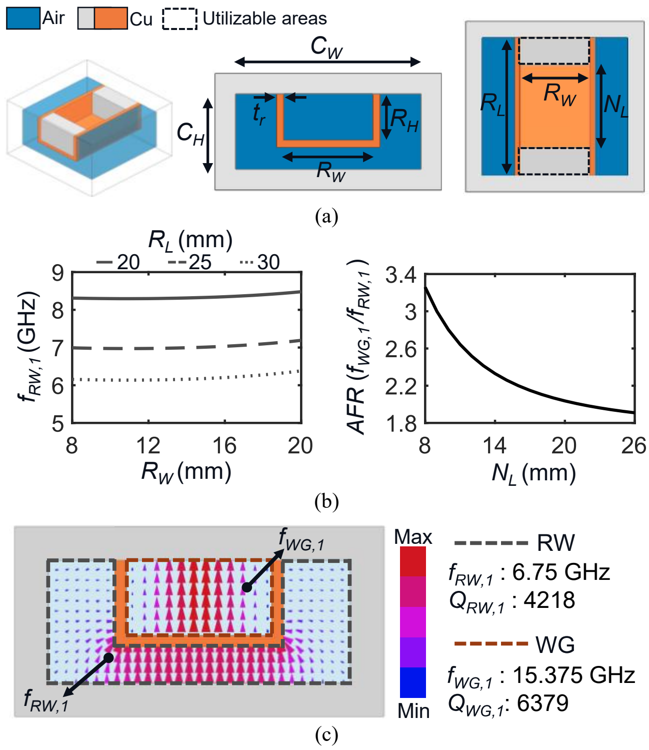

Fig. 2. Proposed RW-WG resonator concept. (a) Bird eye view (left), front view (middle) and top-view (right). (b) $f_{RW,1}$ as a function of R_W and the R_L, and AFR as a function of N_L (right). (c) E-field distribution of the first two fundamental modes $f_{RW,1}$ and $f_{WG,1}$ obtained by eigenmode simulations in ANSYS HFSS. In this example: C_W = 27 mm, C_H = 11 mm, R_H = 6.75 mm, R_W = 13 mm, t_r = 1 mm, R_L = 26 mm, N_L = 14.7 mm.

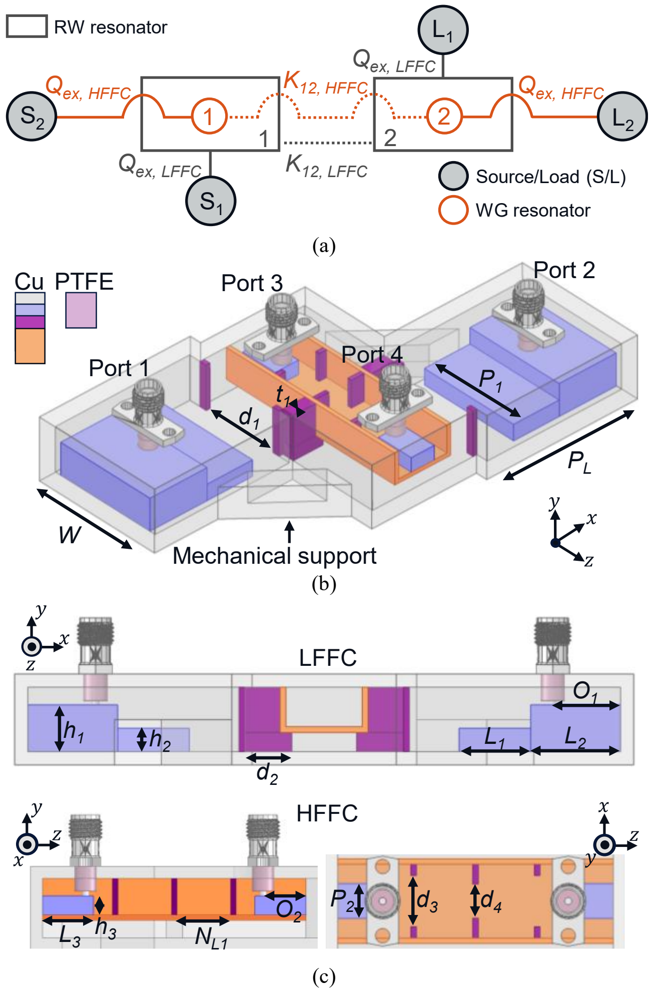

Fig. 3. Nested RW-WG filter concept. (a) CRD, solid lines: external coupling, dotted lines: inter-resonator coupling, grey circles: source/load, orange circles: WG resonator, rectangular: RW resonator. (b) Bird-eye view of the 3D EM simulated model. (c) Details of the LFFC and the HFFC.

the RW and WG resonators and are provided in Fig. 2(b) for a ridge height (R_H)= 6.75 mm. In all of these cases, the length of the WG resonator (N_L) is set to be smaller or equal to the length of the RW resonator (R_L) and the ridge width of the RW resonator (R_W) is bigger than R_H. The analysis shows that $f_{RW,1}$ is more influenced by R_L as opposed to R_W. According to the target working frequency for the LFFC, the dimensions are selected as R_L = 26 mm and R_W = 13 mm. Next, a geometric parametric analysis is performed for $f_{WG,1}$ via the AFR and is provided in Fig. 2(b). As observed, altering N_L allows the targeted resonance frequency of $f_{WG,1}$ to be achieved with an AFR range from 1.91 to 3.26. This configuration allows the adjustment of $f_{WG,1}$ without altering the RW resonator or $f_{RW,1}$. To set $f_{WG,1}$ at 15.375 GHz, an N_L = 14.7 mm is selected. Although a single AFR case is demonstrated, larger or smaller AFRs can be achieved by altering the N_L.

To demonstrate the potential of the proposed nested RW-WG resonator for multi-channel architectures, a dual-channel BPF geometry is designed to have a: i) LFFC with center frequency (f_{cen}) of 6.75 GHz, second-order transfer function with in-band return loss ripple of 25 dB and 7.5% 3 dB-FBW [external coupling ($Q_{ex,\,LFFC}$)= 37 and inter-resonator coupling ($K_{12,\,LFFC}$) = 0.0441] and, ii) a HFFC with f_{cen} of 15.375 GHz, second-order transfer function with in-band return loss ripple of 25 dB and 5% 3 dB-FBW ($Q_{ex,\,HFFC}$ = 30.53 and $K_{12,\,HFFC}$ = 0.038). The coupling routing diagram (CRD) and its corresponding 3D dual-channel geometry are illustrated in Figs. 3(a), (b), (c) respectively. Whereas an in-line SMA-based RF excitation scheme is used for the HFFC, the SMA-based RF ports for the LFFC are set with a 180° offset to suppress the second- and the third- high order modes of the LFFC. Furthermore, they are located at $\lambda_g/4$ distance from the cavity walls. The design process starts by extracting Q_{ex} and K_{12} for the LFFC and the HFFC after performing parametric geometrical studies for each of their relevant dimensions.

The LFFC design is performed using as a reference the parametric studies in Fig. 4(a) which show the dependence of: i) $K_{12,\,LFFC}$ on the inductive iris's length and thickness (d_2, t_1) and of: ii) $Q_{ex,\,LFFC}$—also realized with an inductive iris d_1—on the inductive iris's width when its thickness is 1 mm. Using these parametric studies as a basis, the geometrical dimensions of the LFFC are selected as follows: W = 29 mm, P_1 = 26 mm, h_1 = 8 mm, h_2 = 4 mm, d_1 = 19.5 mm, d_2 = 8 mm, t_1 = 3.05 mm, P_L = 36 mm, L_2 = 15.30 mm, L_1 = 12.20 mm, O_1 = 11.56 mm.

The HFFC is located inside of the hollowed RW resonator, allowing to achieve size compactness by re-using the LFFC volume, shown in Figs 3(b), (c), respectively. Fig. 4(b) shows the dependence of: i) $K_{12,\,HFFC}$ on the inductive iris's width (d_4) and of: ii) $Q_{ex,\,HFFC}$ as a function of an inductive iris's width (d_3)— when its thickness is chosen as 1 mm. Using these studies as a basis, the dimensions of the HFFC are selected as follows: L_3 = 8.4 mm, h_3 = 4.1 mm, N_{L1} = 11.6 mm, O_2 = 5.85 mm, P_2 = 6.25 mm, d_3 = 8.15, d_4 = 5.3 mm.

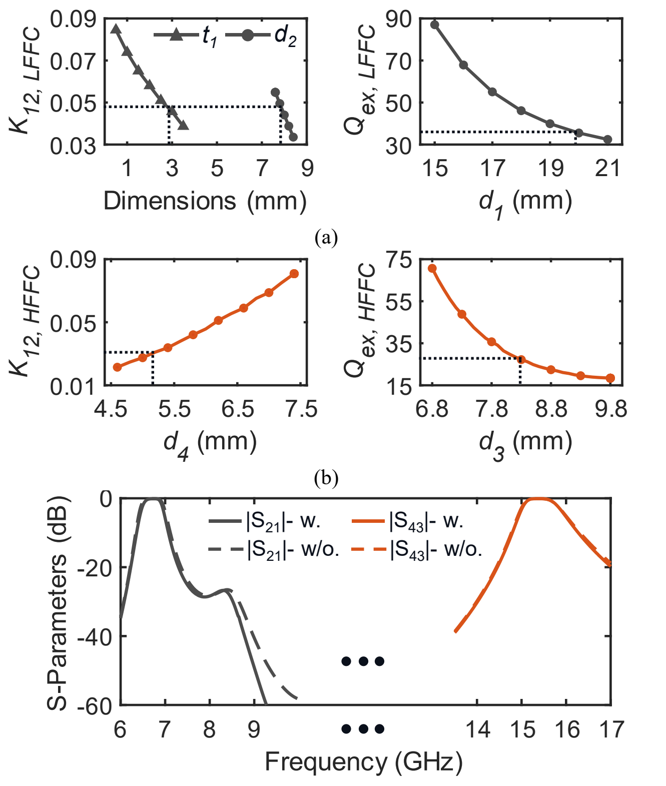

Fig. 4. (a) Extracted $K_{12,\,LFFC}$ as a function of d_2, t_1 and extracted $Q_{ex,\,LFFC}$ as a function of d_1. (b) Extracted $K_{12,\,HFFC}$ as a function of d_4 and extracted $Q_{ex,\,HFFC}$ as a function of d_3. (c) EM S-Parameters simulation with/without adding releasing hole/slots.

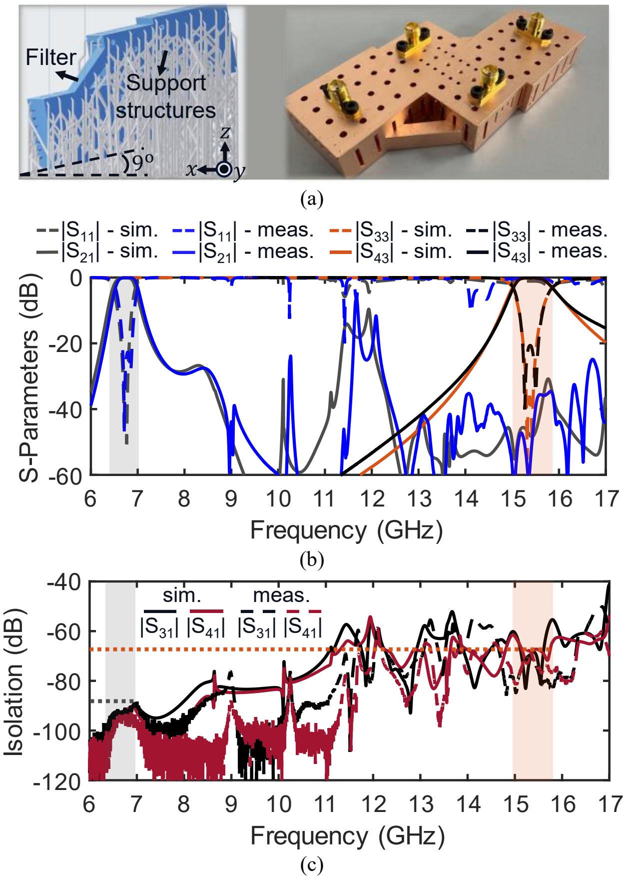

Fig. 5. Second order two-channel nested BPFs. (a) CAD model for SLA-based manufacturing (left). Bird-eye view of the manufactured prototype (right). (b), (c) RF measured and EM-simulated S-parameters.

To facilitate monolithic integration using SLA 3D printing, release holes and slots are added on the filter walls to enable copper plating of the plastic walls using a commercially available wet chemical solution without impacting the performance of the filters. This is achieved by selecting dimensions to be smaller than $\lambda_g/10$ and by placing the slots along current paths to avoid unwanted radiation. For the case of the LFFC, the holes diameter is set equal to 2.25 mm, and the slot dimensions (width x height) are 1.4 mm x 11 mm. Due to the smaller size of the HFFC, its holes have a diameter of 1.5 mm. The EM-simulated performance before and after adding release holes/slots of the overall RW-WG-based BPF are provided in Fig. 4(c). As can be seen, the perforations do not affect the performance of the two channels.

III. Experimental Validation

To validate the dual-channel nested RW-WG BPF concept, a prototype comprising two second-order BPFs was manufactured using SLA 3D printing and a commercially-

Table.1 . Comparison with state-of-the-art multi-channel filters

Ref.	[7]	[8]	[9]	[13]	T.W.
Tech.	CNC	CNC / DR	CNC /DR	Microstrip /SIW	SLA
#N-*#M*	3-3/4/3	2-3/3	12-2	2-2/2	2-2/2
f_{cen} (GHz)	5.8/27/27	1.53/1.68	2.4	11.7/19.1	6.77/15.39
3-dB FBW (%)	1.9/2 &2.3	1.6/1.6	0.6	5.32/4.83	7 /5.3
IL (dB)	0.9-0.6-0.7	0.68-0.68	1.01	0.91-1.22	0.16-0.2
Isolation (dB)	N.A/47/53	30/24.5	25	38.7/45.6	95/71
Vol. (λ_0^3)	0.035	0.027	0.043	1.21 (λ_g^2)	0.17
ICFR	No	No	No	No	Yes

T.W.: This work, DR: Dielectric resonator, *#N*: number of channels, *#M*: order, ICFR: Independent center frequency reconfigurability.

available copper-plating process. Its corresponding CAD model for monolithic 3D printing and its manufactured prototype are provided in Fig. 5(a). As shown, an orientation angle of 9° is applied through the x-z plane, and external support structures are used to aid manufacturing without the need for internal supports that could otherwise affect the performance of the dual-channel BPF. The manufactured prototype has a weight of only 63 g.

Its RF performance was characterized using a Keysight PNA-X network analyzer and provided in Fig. 5(b). It exhibits the following characteristics: i) LFFC: f_{LFFC} = 6.77 GHz, 3 dB-FBW of 7%, minimum in-band IL of 0.16 dB that corresponds to a Q_{eff} of 1,060 and 20 dB upper-stopband up to 11.6 GHz (1.72 ratio of $f_{LFFC,2}$ / $f_{LFFC,1}$) ii) HFFC: $f_{HFFC,1}$ = 15.39 GHz, 3dB-FBW of 5.3%, minimum in-band IL of 0.2 dB that corresponds to a Q_{eff} of 1,365. The isolation between the two different channels was also measured and is provided in Fig. 5(c). As observed, the maximum isolation between the LFFC and HFFC was measured around 95 dB. Finally, a comparison with the EM simulated S-parameters is also shown in Fig. 5(b) and appears to be in good agreement successfully validating the proposed dual-channel RW-WG filter concept.

Lastly, Table 1 presents a comparison between the proposed nested dual-channel RW-WG filter and existing state-of-the-art (SOA) dual/multi-channel filters. To the best of the authors' knowledge, this is the only dual-channel and monolithically-integrated 3D waveguide BPF that is realized using a nested RW-WG resonator approach. It out-performs the SOA in terms of ultra-high channel isolation (> 60 dB), independent channel control and compact size through volume re-use and monolithic SLA-based integration. Furthermore, it also has the lowest IL. The demonstrated channel flexibility makes this concept very promising for emerging multi-standard RFFEs.

IV. Conclusion

This paper presented an ultra-compact dual-channel 3D waveguide filter concept based on a novel nested RW-WG resonator approach. Size compactness is achieved by: i) re-using traditionally unused areas of a ridge waveguide and ii) monolithic integration enabled by stereolithography apparatus 3D printing. For proof-of-concept validation purposes, a dual-channel RW-WG BPF was designed, manufactured and tested. It exhibited a second order low frequency filtering channel at 6.77 GHz with minimum in-band insertion loss (IL) of 0.16 dB (Q_{eff} of 1,060) and 3 dB FBW of 7%, and a second order high-frequency filtering channel at 15.39 GHz with minimum IL of 0.2 dB (Q_{eff} of 1,365) and 3 dB FBW of 5.3%.

Acknowledgment

This work was supported by Research Ireland under Grants 13/RC/2077_P2 and 20/RP/8334.

References

[1] R. V. Snyder, A. Mortazawi, I. Hunter, S. Bastioli, G. Macchiarella and K. Wu, "Present and future trends in filters and multiplexers," in *IEEE Transactions on Microwave Theory and Techniques*, vol. 63, no. 10, pp. 3324-3360, Oct. 2015.

[2] M. Jia, X. Gu, Q. Guo, W. Xiang and N. Zhang, "Broadband hybrid satellite-terrestrial communication systems based on cognitive radio toward 5G," in *IEEE Wireless Communications*, vol. 23, no. 6, pp. 96-106, December 2016.

[3] V. E. Boria and B. Gimeno, "Waveguide filters for satellites," in *IEEE Microwave Magazine*, vol. 8, no. 5, pp. 60-70, Oct. 2007.

[4] Xiao-Peng Liang, K. A. Zaki and A. E. Atia, "Dual mode coupling by square corner cut in resonators and filters," in *IEEE Transactions on Microwave Theory and Techniques*, vol. 40, no. 12, pp. 2294-2302, Dec. 1992.

[5] R. Orta, P. Savi, R. Tascone and D. Trinchero, "Rectangular waveguide dual-mode filters without discontinuities inside the resonators," in *IEEE Microwave and Guided Wave Letters*, vol. 5, no. 9, pp. 302-304, Sept. 1995.

[6] Ji-Fuh Liang, Xiao-Peng Liang, K. A. Zaki and A. E. Atia, "Dual-mode dielectric or air-filled rectangular waveguide filters," in *IEEE Transactions on Microwave Theory and Techniques*, vol. 42, no. 7, pp. 1330-1336, July 1994.

[7] C. Hu, Y. Li and J. Wang, "A Large-Frequency-Ratio multichannel bandpass filter based on structure-shared mode-composite air-filled cavity resonators," in *IEEE Transactions on Microwave Theory and Techniques*, vol. 72, no. 6, pp. 3650-3661, June 2024.

[8] L. Xu, W. Yu, W. Qin and J. -X. Chen, "Design of dual-channel filter based on dual-mode dielectric resonators," in *IEEE Transactions on Circuits and Systems II: Express Briefs*, vol. 69, no. 1, pp. 45-49, Jan. 2022.

[9] J. -X. Xu, X. Y. Zhang, H. -Y. Li, Y. Yang, E. Dutkiewicz and Q. Xue, "Ultracompact multichannel bandpass filter based on trimode dielectric-loaded cavities," in *IEEE Transactions on Microwave Theory and Techniques*, vol. 68, no. 5, pp. 1668-1677, May 2020.

[10] C. Guo, X. Shang, M. J. Lancaster and J. Xu, "A 3-D printed lightweight X-Band waveguide filter based on spherical resonators," in *IEEE Microwave and Wireless Components Letters*, vol. 25, no. 7, pp. 442-444, July 2015.

[11] K. Zhao and D. Psychogiou, "Monolithic SLA-Based capacitively-loaded High-Q coaxial resonators and bandpass filters," 2020 *50th European Microwave Conference (EuMC)*, Utrecht, Netherlands, 2021, pp. 471-474.

[12] E. López-Oliver and C. Tomassoni, "3-D-Printed dual-mode filter using an ellipsoidal cavity with asymmetric responses," in *IEEE Microwave and Wireless Components Letters*, vol. 31, no. 6, pp. 670-673, June 2021.

[13] G. Zhang et al., "Multilayer packaged single- and dual-band dual-channel bandpass filters based on substrate integrated waveguide cavities," in *IEEE Transactions on Components, Packaging and Manufacturing Technology*, vol. 14, no. 1, pp. 114-121, Jan. 2024.